Cold Regions Science and Technology 215 (2023) 103967

Contents lists available at ScienceDirect

Cold Regions Science and Technology

journal homepage: www.elsevier.com/locate/coldregions

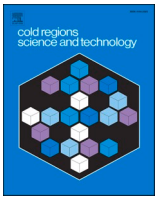

Characterization of hollow glass microspheres with potential for regional climate intervention to preserve snow and ice surfaces

Julia Farkas [a,*], Marianne Molid [a], Bjørn Henrik Hansen [a], Tor Nordam [a], Trond Nordtug [a], Patricia A. Carvalho [b], Mimmi Throne-Holst [a]

[a] SINTEF Ocean, Department of Climate and Environment, Trondheim, Norway
[b] SINTEF Industry, Department of Material Physics, Oslo, Norway

ARTICLE INFO

Keywords:
Hollow glass microspheres
Ice and snow
Climate intervention
Albedo
Environmental fate

ABSTRACT

Cold regions including the Arctic are warming fast, resulting in increased losses of snow and ice cover. A climate intervention approach, where hollow glass microspheres (HGMs) are applied on snow and ice surfaces such as Artic sea ice has been suggested for ice preservation. HGMs are commercial materials, typically in the 10–200 μm diameter size range. They are very lightweight, highly reflective materials with a high crush strength. It is suggested that through that reflectivity, their application onto snow and ice surfaces can increase the albedo, and thus stabilize snow and ice covers, for example aid the formation of multiyear sea ice. In this study we tested the stability and behaviour of different HGMs under stress conditions to gain knowledge on their potential environmental fate. Stability tests, measured as maintenance of positive buoyancy, during sediment interaction, repeated freezing and thawing and prolonged exposure in seawater showed differences in environmental stability of the tested materials with stability depending on wall thickness and surface integrity. None of the tested materials seemed to be very susceptible to biofouling under the conditions tested. However, leaching of elements, especially Si was observed for some materials, potentially indicating dissolution of the HGMs in seawater over time. Further studies are needed to determine the element dissolution from HGMs and other potential environmental implications such as impacts on organisms. Although this paper is directed towards using HGMs in a local climate intervention application the findings may be of general interest for other uses of HGM materials.

1. Introduction

The Intergovernmental Panel on Climate Change (IPCC) continuously assesses the impacts and future risks connected to global warming (see e.g. Intergovernmental Panel on Climate Change, 2018, 2021, 2022). The panel has also evaluated the role of, and impacts on, the ocean and cryosphere in a changing climate (Intergovernmental Panel on Climate Change, 2019) and thoroughly analysed strategies for mitigation of climate change (Intergovernmental Panel on Climate Change, 2022). These reports summarise the scientific grounds for the on-going and future anthropogenic climate change, its potential impacts and the urgent need for climate change mitigation action and restoration of natural environments. The primary climate change mitigation strategy is reduction in emissions of CO_2 to the atmosphere. However, there is a growing and urgent concern that emissions are not being sufficiently reduced in time to meet international targets such as the Paris Agreement of limiting global warming to well below 2 °C, preferably to 1.5 °C, compared to pre-industrial levels. A major concern is that climate tipping points, such as massive loss of Arctic and Antarctic ice, with potentially catastrophic consequences, will be reached if serious action is not taken.

White snow and ice have a high albedo and thereby play an important role in regulating the global climate through reflecting incoming solar radiation back into space. A decrease in the snow and ice surface, e.g. the polar caps, of the earth will decrease the earth's albedo and thereby increase the planet's surface temperature since more solar energy gets absorbed by the exposed water or land (Perkins, 2019). This will in turn accelerate further loss of snow and ice, causing a positive feedback loop and further increased surface temperature. The planetary warming caused by a decrease in ice cover in the Arctic is substantial and Pistone et al. (2014) estimated that the effect of this albedo change, if averaged globally, is equivalent to 25% of the direct climate forcing from CO_2 during the past 30 years. Notz and Stroeve (2016) have shown that the loss of Arctic summer (September) sea ice is directly coupled to

* Corresponding author at: SINTEF Ocean, Brattørkaia 17C, 7010 Trondheim, Norway.
E-mail address: julia.farkas@sintef.no (J. Farkas).

https://doi.org/10.1016/j.coldregions.2023.103967
Received 23 February 2023; Received in revised form 29 June 2023; Accepted 17 July 2023
Available online 10 August 2023

CO_2 emissions in a linear relationship. Furthermore, Stroeve et al. (2012) reported that a seasonally ice-free Arctic Ocean within the next few decades is a distinct possibility.

As climate intervention approach, Field and co-workers have suggested the application of a very thin layer of hollow glass microspheres (HGMs) on top of first-year Arctic ice to increase its albedo and thereby slow the ice melt could potentially restore multi-year ice over time (Field et al., 2018). Further, using HGMs to for aiding the stabilization of local ice and snow covers that are important for infrastructure such as the ice pier at the McMurdo Station in Antarctica, or pipelines and roads in permafrost areas is contemplated (Wolff, personal communication).

However, climate intervention is controversial for several reasons. There are socio-political concerns relating to the ethical and moral justifications of intervening with the natural climate system of the world (Bennett et al., 2022). There is also a concern that climate intervention would undermine essential efforts to reduce CO_2 emissions. In addition, there are concerns relating to the economic feasibility as well as the physical and environmental safety of climate intervention approaches (Keith, 2000).

Before considering the economic and technical feasibility of application og HGMs for ice conservation, it is necessary to understand the fate and potential effects of HGMs in the environment, especially cold ecosystems like the Arctic.

The aim of this work was to study the integrity of four types of HGMs that are considered to be used for climate intervention approaches under cold-climatic conditions. In particular we tested interaction with sediments, cycles of freezing and thawing in sea ice and during interactions with natural microfauna in cold sea water over time. This helps to select potentially feasible HGM candidates for climate intervention, and also forms the basis for future environmental assessment studies with selected materials.

2. Material and methods

Four HGMs were characterized and then evaluated under four stress conditions: weathering HGMs with sediment; a frazil ice freeze/thaw study; a biofouling experiment; and a study to determine if leaching of elements from HGMs into seawater occur. These studies are described below.

2.1. HGM materials used

Four different HGM materials were selected from a range of available HGMs by the Arctic Ice Project based on their size, reflectivity, and availability to be tested in this study this study, namely: Sphericel 25P45 and Q-Cel 300 (Potters Industries LLC, UK), Glass Bubbles K1 (3 M, USA) and Porasphere 90–180 (Dennert KG, Germany). Hereafter the materials will be referred to as 25P45, Q-Cel, K1 and PS, respectively. The net reflectivity was previously determined by the AIP (see SI for dry and wet spheres, showing that PS was with 38% net-reflection the most reflective HGM when dry, while 25P25 was, with 28.8% the most reflective material when wet (with results given in SI Table 1). Other key features and characteristics for these materials, as given by their manufacturers, are shown in Table 1.

2.2. Initial HGM material characterization and preparation of materials

Images of the dry and wet materials were taken using a microscope (EclipseNi, Nikon, Japan), and scanning electron microscope (SEM) images of dry HGMs were additionally taken with to verify the wall thickness of the tested materials (see Section 2.2.1). For SEM imaging, the HGMs were deposited on carbon tape and subsequently carbon coated. The observations were carried out with a Field Electron Gun scanning electron microscopy (FEG/SEM) FEI NANOLAB 600 operated at 5 kV.

For this study, stability of the HGM materials was determined as a maintained positive buoyancy and calculated as the relative mass of floating vs sinking HGMs for each tested material. As direct manipulation and handling of the buoyant HGMs could lead to a loss or breakage, the buoyant HGM mass at the start of each experiment was determined by subtracting the mass of the removed, non-buoyant fraction from the total mass. The non-buoyant fractions were removed and collected following phase separation through floatation and thereafter quantified gravimetrically as described in more detail in Section 2.2.2.

2.2.1. Mathematical approximation of HGM properties

To better understand how the different HGM materials may behave in a marine environment we calculated estimates of some key properties for the different materials used here, i.e., HGM wall thickness and their density as a function of size. Wall thickness was further measured from SEM images to verify the calculations.

Information of wall thickness and density can be used to predict approximately which size of HGMs will be positively buoyant (floating), neutrally buoyant (in the water column) and negatively buoyant (sinking).

The effective density of a HGM (assuming the density of air to be 0) is

$$\rho_{eff} = \rho_{glass}\frac{\frac{4\pi}{3}r_2^3 - \frac{4\pi}{3}r_1^3}{\frac{4\pi}{3}r_2^3}. \quad (1)$$

Here, r_1 is the inner radius and r_2 is the outer radius of the glass shell. Solving for r_1, we find

$$r_1 = r_2\sqrt[3]{1 - \frac{\rho_{eff}}{\rho_{glass}}}, \quad (2)$$

and the wall thickness, h, can be found as.

$$h = r_2 - r_1. \quad (3)$$

Calculated values are shown in Table 2 below.

As a simplification, we here assume that the spheres have a range of outer diameters, r_2, but constant wall thickness, h. Given this, we can find the minimum size of spheres of each HGM material that will have a density equal to water, i.e. have neutral buoyancy.

Consequently, spheres that are smaller than this will sink and spheres that are larger than this will float, i.e. have positive buoyancy.

We rewrite the equation for effective density slightly:

$$\rho_{eff} = \rho_{glass}\frac{r_2^3 - (r_2 - h)^3}{r_2^3}. \quad (4)$$

This equation is solved graphically (Fig. S1) by plotting effective density as a function of outer radius, r_2.

Table 1
Description of the tested HGM materials as given by the manufacturers, with D50 (μm) representing the median size. *represents the size range.

Material	Abbreviation	Vendor	D50 (μm)	Crush strength (psi)	Density (g/cc)	Material
Sphericel 25P45	25P45	Potters	47	750	0.25	Borosilicate glass
Q-Cel 300	Q-Cel	Potters	90	500	0.21	Borosilicate glass
Glass Bubbles K1	K1	3 M	65	250	0.125	Soda-lime borosilicate glass
Porasphere 90–180	PS	Dennert	90–180*	2900	0.63	Recycled glass

Table 2
Sphere properties. BSG: Borosilicate glass, SLBSG: Soda-lime borosilicate glass, RG: Recycled glass.

Abbreviation	Material	D_{50} [μm]	ρ_{eff} [kg/L]	ρ_{glass} [kg/L]	r_1 [μm]	h [μm]
25P45	BSG	47	0.25	2.23	22.59	0.91
Q-Cel	BSG	90	0.21	2.23	43.54	1.46
K1	SLBSG	65	0.125	2.375[†]	31.92	0.58
PS	RG	90*	0.63	2.4	60.99	6.51

[†]Note that we could not find the density data for soda-lime borosilicate glass, so the density used is the average of soda-lime glass and borosilicate glass. *We don't have the median diameter for the PS material and have used the average of the distribution range for the calculations.

2.2.2. Measurement of buoyant fractions of HGM materials

To determine the relative amount of positively buoyant HGMs in each material (as received), buoyant and non-buoyant phases were separated by floatation. In detail, pre-weighed amounts of HGMs (depending on the material between 50 and 415 mg) were added to separating funnels filled with approximately 50 mL MilliQ water (Milli-Q® IQ 7003, Merck, Germany). The funnels were then swirled repeatedly before being left for at least 1 h at room temperature to enable phase separation of the HGMs. The non-buoyant phase was then collected into 50 mL centrifuge vials and transferred onto preconditioned (rinsed with MilliQ water) and pre-weighed fibre glass filters (GF-C, Whatman, UK). To minimize material losses, the vials were rinsed repeatedly, and the material collected onto the same filter. The samples were then dried for at least 24 h at 50 °C and weighed. Similarly, the buoyant HGMs were rinsed out of the funnel, collected, dried and weighed. A mass balance was established and the relative amounts (mass based) of positively and negatively buoyant HGMs determined. In this first investigation MilliQ water was used for floatation to avoid interference with salt precipitates from seawater in gravimetric mass determination. In later experiments filtered seawater was used thereafter for preparing buoyant HGMs for experiments to avoid dilution of seawater as flushing filters with MilliQ water was found to be sufficient to remove salt precipitates.

2.3. Weathering of HGMs in interaction with sediment

HGMs may be broken when suspended with sediments in sea water. We therefore assessed whether and how fast this may occur, and if any of the HGMs were more resistant to breaking under the tested conditions. Initial trials were performed to optimize the method with respect to amount of HGMs, sand and seawater and shaking speed and time to ensure HGM suspension and interaction with sediment. In the final setup, 10 g of aquarium sand was added per Erlenmeyer flask (250 mL) before filtered seawater (20 mL) was added. The sand had a grain size of ≤0.5 mm (Specialsand, Rådasand AB, Sweden) and was washed in regular tap water and MilliQ water to remove dust and impurities, and then dried before use. Then, 240 ± 10 mg, 230 ± 10 or 220 ± 10 mg of 25P45, K1 or PS, respectively, were added to the flasks ($N = 3$). The buoyant fraction of each HGM material to be tested was prepared by floatation as described above. In addition, one sample per material ($N = 1$) was prepared in the same way but without addition of sand to determine if there is any loss of HGMs in the absence of sediment.

The flasks were placed on a rotary shaking table (Infors HT Orbitron, Switzerland) at 100 rpm and 10 °C. After 24 and 48 h, three replicates of each HGM material containing water and sand, and one sample containing HGMs and water only, were sampled by decanting them into separatory funnels leaving the sand in the flasks. To collect remaining (buoyant) HGMs, each flask with sand was rinsed three times with approximately 10 mL MilliQ water that were also added to the funnels. After a settling time of at least 1 h, the bottom fraction was removed from the funnels. Subsequently, the top fraction, containing the buoyant HGMs was collected into 50 mL centrifuge tubes by repeated rinsing and filtered onto preconditioned and pre-weighed filters as described above. After drying, the mass of buoyant HGMs at both time points was determined gravimetrically.

2.4. Effect of cycles of freezing and thawing on HGMs

As HGMs may be exposed to freezing-thawing cycles during application in the cold environments, such as the Arctic, we assessed the stability of HGMs during repeated cycles of freezing and thawing. Frazil sea ice was prepared by filling sterile filtered seawater into metal trays at −20 °C under regular stirring. A total of 45 beakers were prepared with frazil sea ice (200 mL), and intact buoyant HGMs, 225 ± 20 mg, 210 ± 20 mg or 230 ± 17 mg of 25P45, K1 or PS, respectively, were added to the ice surface (15 beakers for each material). The beakers were then frozen at −20 °C. Each week, all beakers were placed at room temperature overnight to thaw. Three replicates of each material were then sampled, and the remaining replicates were placed back at −20 °C to undergo further freezing-thawing cycles. Five freezing-thawing cycles were performed within 5 weeks. Immediately after thawing, the samples were washed into separatory funnels, where buoyant and non-buoyant HGMs were separated and collected into centrifuge tubes. Both buoyant and non-buoyant HGMs were collected on pre-weighed fibre glass filters, dried at 50 °C for at least 48 h and weighed as described above to determine the relative amount of buoyant HGMs.

2.5. Biofouling of HGMs

To test possible biofouling of HGMs under relevant conditions, unfiltered natural sea water (20*L*) was collected from the Trondheimsfjord, outside the harbour area of Trondheim, 63°26′N, 10°26′E, in January 2022 (salinity 31.84 ppt, pH 7.72). The water was left in a temperature-controlled room to reach 10 °C before being filled into flat glass bottles (1 L). Subsequently, 251 ± 11 mg (25P45), 228 ± 10 mg (K1) or 214 ± 3 mg (PS), respectively, of buoyant and washed HGMs were added. The bottles were incubated on carousel systems (Brakstad et al., 2015) at 15 rpm and 10 °C for three months.

The content of each bottle was then separated into the positively buoyant phase (surface), the neutrally buoyant phase (water column) and the negatively buoyant phase (bottom). From each phase small aliquots were sampled for determination of the occurrence of microorganism using DAPI staining (D9542, Sigma-Aldrich) followed by cell counting using an epifluorescence microscope (EclipseNi, Nikon, Japan). The rest of the samples were used to obtain a mass balance between positively, neutrally and negatively buoyant HGMs. As non-biofouled controls, samples incubated in the same way, but in sterile filtered seawater (see leaching of elements below) were used.

2.6. Leaching of elements from HGMs

To study the leaching of elements from HGMs in seawater, 236 ± 11 mg of buoyant 25P45, 223 ± 13 mg of buoyant K1 or 312 ± 20 mg of buoyant PS were added to acid washed (soaked in 1 M analysis grade HNO_3 overnight, subsequently soaked and rinsed three times with MilliQ water) 250 mL glass bottles, which were then filled to the rim (total filling volume 307 mL) with sterile filtered sea water ($N = 3$). The bottles were incubated on carousel systems (Brakstad et al., 2015) at 15 rpm and 10 °C for three months. At termination of the experiment, a 10 mL sample was taken from each bottle, filtered through a 45 μm polyethersulfone filter (VWR International, Radnor, USA) into a metal free centrifuge tube and acidified immediately with three drops of ultrapure 65% HNO_3. The samples were then analysed for concentrations of the elements Al, Si, Ca, Cr, Fe, Zn, La and Pb, using an Agilent 8800 Triple Quadropole ICP-MS (ICP-QQQ) equipped with an SPS 4 autosampler using standards from Inorganic Ventures (Christiansburg, USA). The concentrations were then converted into μg/L leached per g/L of HGM.

The rest of the samples were used as sterile filtered controls for the

biofouling experiment. The content of each vial was transferred to a flat bottle, that was then filled completely with sterile filtered sea water. The content was separated into buoyant phase (surface), the neutrally buoyant phase (water column) and the negatively buoyant phase (bottom), and gravimetrically analysed as described above for the biofouling experiment.

2.7. Statistics

Data analyses were performed with GraphPad Prism 9 (Graph-Pad Software Inc., USA). To determine statistical differences between groups, data sets were analysed with one-way ANOVA and associated post-hoc tests.

3. Results

3.1. HGM material characterization and selection for further studies

Scanning and light microscopic images of the dry materials are shown in Fig. 1A-D. The 25P45 and K1 HGMs looked similar, with 25P45 HGMs appearing to be slightly smaller in size. The PS HGMs were relatively thick-walled with pores (Fig. 1D, insert). The Q-Cel sample contained non-spheric particulate material and needle-like structures (Fig. 1B).

The relative mass-based amount of positively buoyant HGMs in the materials as received is presented in Fig. 1E. The data show that K1 and Q-Cel contained, with 87 ± 0.9% and 88 ± 2%, respectively, the highest relative amount of positively buoyant spheres at start. The 25P45 batch contained 73 ± 1% positively buoyant HGMs, while replicates from the batch of PS had a large variability with, on average, 66 ± 20% positively buoyant HGMs. The negatively buoyant fraction contained pieces of broken spheres and spheres that either had holes or cracks and had thus filled with water. Small, seemingly whole, spheres were also observed in the negatively buoyant fraction. Images are shown in the supporting information (Fig. S2). Calculations of HGM density as a function of radius indicated that spheres with a diameter of approximately <9.84 µm for 25P45, <15.74 µm for Q-Cel, <6.76 µm for K1 and < 76.90 µm for PS, respectively, will be negatively buoyant in seawater.

3.2. HGM weathering in interaction with sediment and natural sea water

To assess the potential effect of weathering, the amount of positively buoyant HGMs of three HGM materials (excluding Q-Cel) was determined after 24 and 48 h of interaction with sediment (Fig. 2; bars with

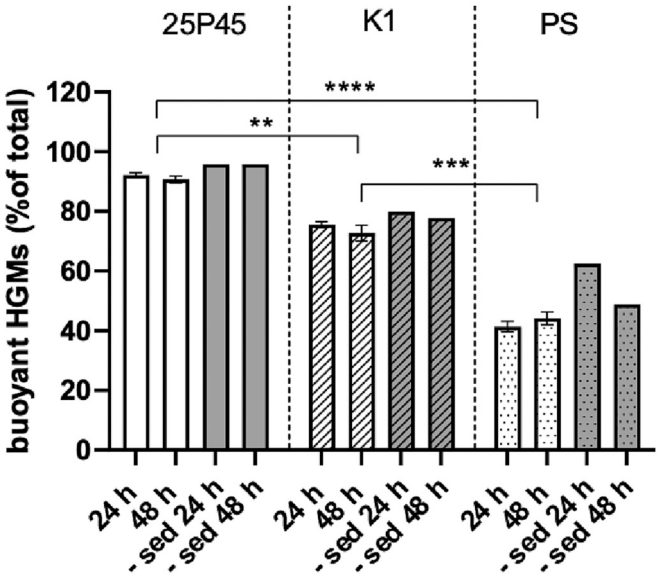

Fig. 2. Recovery of buoyant HGMs after 24 and 48 h of shaking at the water-sediment interphase (bars with white background), and in seawater without sediment (bars with grey background). Data shown as mean ± SD for sediment containing samples ($N = 3$). Stars indicate statistically significant differences (**$p < 0.01$; ***$p < 0.001$; ****$p < 0.0001$) between groups.

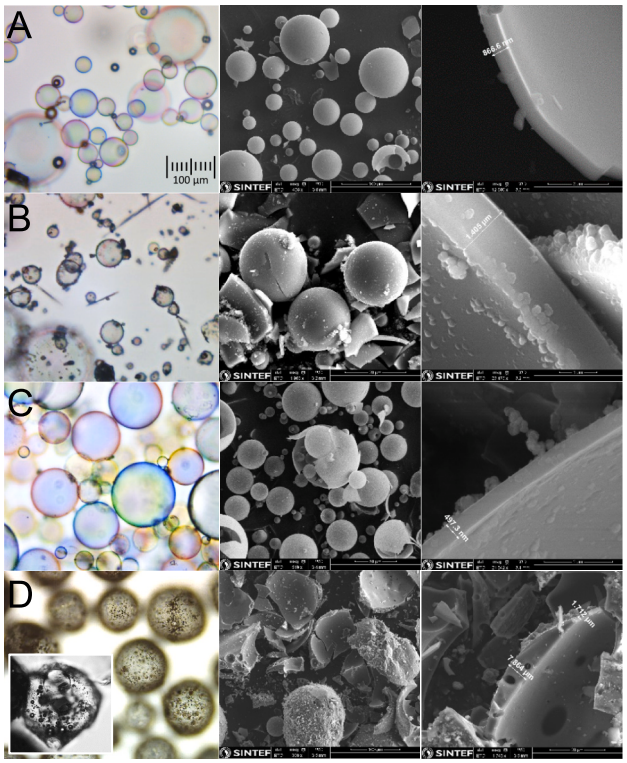

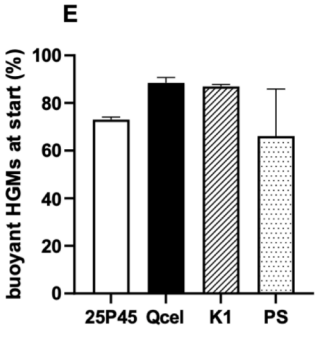

Fig. 1. Light and scanning electron microscope images of dry samples of HGM materials row A: 25P45; row B: Q-Cel; row C: K1 and row D: PS. The scale bar (100 µm) as shown in A is the same for all light microscopy images (left column). The SEM images in the middle column show whole and fragmented HGMs, with the right row showing the shell thickness. Not the different scale bars. E) The relative amount (% of total) of positively buoyant HGMs of the respective materials as they were received. Data presented as mean ± SD ($N = 3$).

white background). Results show that 25P45 was the most stable material with 92.2 ± 0.8% of the added HGMs being recovered as positively buoyant material.

from the water surface after 24 h interaction with sediment, which was also the case for this material after 48 h interaction with sediment (90.7 ± 1.1). For K1, recovery of positively buoyant material was significantly ($p = 0.0077$) lower than for 25P45, with 75.5 ± 1 and 72.7 ± 2.61% buoyant material recovered at 24 and 48 h, respectively. PS was the material with the lowest recovery of positively buoyant HGMs after interaction with sediment, which was 41.4 ± 1.74% after 24 h and 44.1 ± 2.11% after 48 h. Recovery of positively buoyant HGMs of all materials incubated without sediment was higher than in sediment groups with, 95.7% (24 and 48 h) for 25P45, 79.9% (24 h) and 77.8% (48 h) for K1, and 62.4% (24 h) and 48.9% (48 h) for PS, (Fig. 2; bars with grey background).

3.3. Stability under freezing and thawing cycles

HGMs spread on ice, for example Arctic sea ice, can be subjected to repeated freeze/thaw cycles throughout the year. The three HGM materials 25P45, K1 and PS were tested for their stability under repeated (x5) freezing and thawing conditions. Samples from five weekly timepoints (TP) were examined for the occurrence of positively buoyant material (Fig. 3). The 25P45 material was the most stable material under the tested conditions, with similar recoveries of buoyant HGMs throughout the experiment, which was between 94.5 ± 1.3% (TP5) and 95.6 ± 0.8% (TP2). Overall recovery rates of buoyant K1 material was less than for 25P45 ($p = 0.0019$) but was also stable over time, reaching from 74.7 ± 1.5% (TP3) to 78.5 ± 0.5% (TP4). Recovery of buoyant PS material was less than for both 25P45 and K1 ($p < 0.001$) and decreased significantly ($p < 0.001$) over time, as demonstrated through a decrease from 61 ± 1 at TP1 to 36 ± 1% at TP5. The decrease in buoyant PS material was largest between TP1 and TP2, and seemed to stabilize between TP3 and TP5, indicating that a portion of the materials is less resistant to cycles of freezing and thawing.

3.4. HGMs susceptibility to biofouling and effects on buoyancy

HGMs were incubated in natural sea water at 10 °C without added nutrients to simulate water column conditions relevant for cold climatic areas. All materials were incubated for three months under these conditions and then examined for potential biofouling and mechanical breakage.

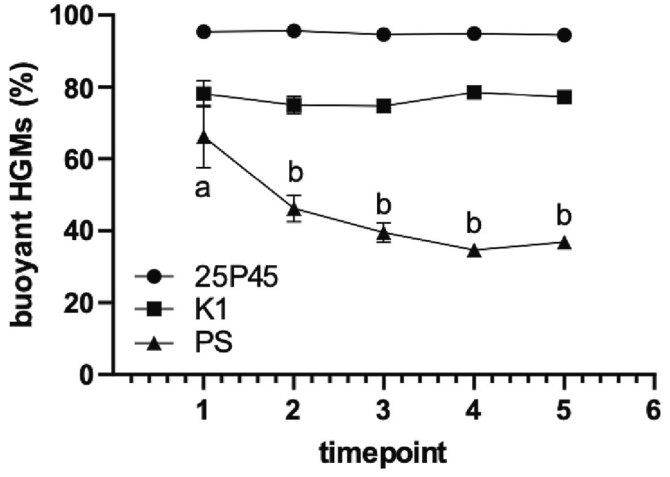

Fig. 3. Relative amount (%) of recovered buoyant HGMs after repeated freezing and thawing cycles (each timepoint representing one week of freezing). 25P45 is depicted as circles, K1 as squares and PS as triangles. Data are shown as mean ± SD ($N = 3$). Significant differences between timepoints for the same material are depicted as different letters ($p < 0.05$).

Weathering of HGMs through e.g. biofouling and/or mechanical breakage in turbulent water masses may cause the HGMs to lose their positive buoyancy. The relative distribution (% total recovered) of positively buoyant (surface), neutrally buoyant (water column) and negatively buoyant (bottom) HGMs of each of the tested materials, 25P45, K1 and PS, was determined after incubation in natural non-filtered and sterile filtered seawater for 3 months (Fig. 4). In non-filtered seawater, the total mass-based recovery of originally added material was 83 ± 0.84% for 25P45, 43 ± 3% for K1 and 107 ± 0.8% for PS. In sterile filtered seawater total recovery was higher for 25P45 (92 ± 2%) and for K1 (77 ± 4%) and was similar for PS (104 ± 3%).

The results show that, almost all (95 ± 0.4%) of the recovered 25P45 HGMs were positively buoyant, with 1% being neutrally buoyant, and 3 ± 0.1% negatively buoyant (Fig. 4A) in exposures containing natural non-filtered seawater. For K1 and PS, only 34 ± 2 and 26 ± 6% of the HGMs were positively buoyant. While some K1 HGMs were neutrally buoyant (20 ± 3%), most of the PS HGMs (71 ± 5%) were negatively buoyant at the end of the experiment (Fig. 4A).

The buoyancy distribution of 25P45 and PS HGMs were relatively similar after incubation in sterile filtered seawater as compared to in non-filtered seawater, however, more K1 HGMs were found to be positively buoyant in the sterile filtered seawater exposure compared to non-filtered natural seawater.

DNA staining with DAPI revealed the presence of bacteria in all non-filtered natural seawater samples. In control flasks, the determined bacterial number, 206373 ± 50,030, 189,333 ± 44,210 and 205,427 ± 30,367 bacterial cells/mL, was similar in all three sampled compartments, surface, water column and bottom.

In most HGM samples, no bacterial growth was detected directly on the sphere surfaces. Further, in samples/phases containing many HGMs, the presence of spheres complicated or hindered direct cell counts due to shading caused by intact HGMs, thus bacterial numbers could not be quantified for all samples. For 25P45, bacterial counts were determined for the water column and the bottom samples, resulting in a bacterial count of 104,133 ± 3279 and 95,613 ± 11,478 cells/mL, respectively, which is significantly lower than in controls ($p < 0.05$). For K1 and PS, counting of bacteria was only possible for water column samples. Results show that for K1, the water phase contained less bacteria than in controls (121,173 ± 9129 cell/mL; $p = 0.046$), while numbers for PS were similar to controls (171,347 ± 24,154 cells/mL; $p = 0.83$). Bacteria could be seen in association with the spheres in the bottom phase for K1, but not in the top phase. In PS, bacteria were detected in the surface sample in vicinity to spheres and were also detected on the spheres surface in the bottom phase.

3.5. Element leaching from HGMs during prolonged incubation in sea water

After a three months incubation period in sterile filtered seawater (under rotation at 10 °C), the dissolved concentrations (<0.45 μm) of Al, Si, Ca, Cr, Fe, Zn, Ba, La, Pb were determined. Concentrations are shown in Table 3. Released Ca concentrations were not significantly different from background Ca concentrations in seawater for any of the tested materials (data not shown).

The results indicate that all HGM materials tested leached Al, Si, Fe and Ba, as showed by increased concentrations of these elements in all seawater samples exposed to HGMs as compared to the unexposed seawater (subtracted as background). The 25P45 material further released Zn (375 ± 9 μg/L) and Ba (171 ± 4.9 μg/L) (Table 2). La was only found in samples after exposure to 25P45, however at low concentrations (0.1 ± 0.0045 μg/L). Further, PS released low concentrations of Pb (Table 3).

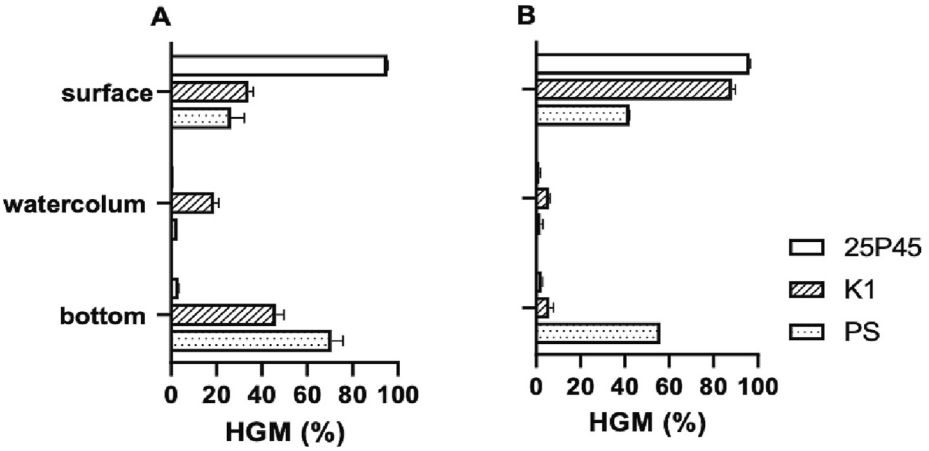

Fig. 4. Distribution of HGMs in the water column, surface (positively buoyant HGMs); water column (neutrally buoyant HGMs) and bottom (negatively buoyant HGMs) A) after incubation, under rotation on carousel systems, in un-filtered natural seawater for three months, B) after incubation, under rotation on carousel systems, in sterile filtered seawater for three months. Data are shown as mean ± SD ($N = 3$).

Table 3
Element concentrations determined in filtered samples taken from the water phase after three months of incubation in sterile filtered seawater. Concentrations are given in μg/L for all elements except Si for which concentrations are given in mg/L. Concentrations were calculated for a release from 1 g/L HGM material. Background levels of the seawater controls were subtracted. Fields with "BG" indicate that levels were similar to background levels.

Material	Al (μg/L)	Si (mg/L)	Cr (μg/L)	Fe (μg/L)	Zn (μg/L)	Ba (μg/L)	Pb (μg/L)
25P45	1.5 ± 1.6	13 ± 0.4	BG	8.2 ± 1.9	375 ± 9	171 ± 4.9	BG
Q-Cel	1.3 ± 0.5	64 ± 1.7	BG	22 ± 12	BG	4 ± 0.5	BG
K1	5.2 ± 1.3	58 ± 3.4	4.1 ± 0.2	9.9 ± 1.7	0.5 ± 1.2	2.7 ± 0.2	BG
PS	89 ± 4.5	0.24 ± 0.01	BG	3.1 ± 1.6	1.6 ± 2.8	7.8 ± 0.1	0.7 ± 0.03

4. Discussion

In this study we examined the stability of HGM materials under varying environmental stress conditions. We here defined stability as the maintenance of a positive buoyancy in (sea)water, since we believe this is an important property for the envisioned climate intervention approach applying HGMs onto ice surfaces, especially on large water bodies such as the Arctic ocean, to increase the albedo and prevent ice melting.

An initial determination of the relative amount (mass based) of positively buoyant HGMs in the materials as they were received revealed that K1 and Q-Cel contained the highest percentage, >85%, positively buoyant spheres. However, due to the occurrence of non-spherical particulate material and needle like structures in Q-Cel samples (Fig. 1B), it was decided to not continue to work with this material as we do not believe that these structures are beneficial to the proposed application. All "as received" HGM batches contained some broken spheres (Fig. S1), that partially accounted for the non-buoyant fraction. However, the sinking fraction of the HGMs did not contain only broken spheres. Many spheres in this fraction still appeared to be whole. Such spheres were filled with water either through (partly visible) holes or potentially micro ruptures or were too small to maintain a positive buoyancy. We estimated that, based on the assumed glass density and calculated wall thickness of the different materials (which was confirmed by SEM images), they would be negatively buoyant at <9.84 μm for 25P45, <15.74 μm for Q-Cel, <6.76 μm for K1 and < 76.90 μm for PS, respectively (Fig. 1). A fraction of small, negatively buoyant but still intact spheres may account for the, in comparison to K1 and Q-Cel, lower amount of positively buoyant 25P45 spheres in the materials as they were received. Our calculations should be regarded as approximations intended to aid the understanding of the observed behaviour of the materials.

The 25P45 material was the most stable material under all tested conditions, followed by K1, which was less stable, and PS, that was most prone to lose positive buoyancy in the conducted experiments. In sediment interaction experiments, the higher stability of 25P45 compared to K1 may be related to the higher isostatic crush strengths as reported by the producer, 750 psi for 25P45 compared to 250 psi for K1, with higher crush strength likely being related to larger wall thickness.

The high density, crush strength and wall thickness did in the case of PS not improve the stability, as PS was found to be the HGM material most prone to sink following exposure to both sediment and seawater only. While the initially sinking HGM fraction was removed before the experiments, it is possible that air was trapped in the porous structure of PS, or that small pores can cause "delayed" entry of water, meaning that trapped air will be slowly replaced by water. It is also possible that the uneven surface structure makes the PS material more susceptible to environmental impacts. On SEM images we also observed that the wall thickness of PS varies (Fig. 1, row D).

The amount of recovered buoyant HGMs did decrease slightly, but not significantly between the 24 and 48 h sediment interaction for all HGMs tested, indicating that the HGMs breakage occurs relatively rapidly. However, longer-term investigations for HGMs selected for further study or potential environmental application are recommended to determine potential wear over time.

We further observed that all tested materials had slightly lower recoveries of positively buoyant HGMs in setups containing sediment, in comparison to no-sediment controls (only seawater), indicating that interaction with sediment did affect the materials. Further, recoveries of K1 and PS were lower than for 25P45 in tests containing only seawater, showing their generally higher susceptibility towards environmental weathering.

Similar to the results of the sediment interaction study, K1 and PS had a lower stability compared to 25P45 under freezing-thawing conditions, which, even after 5 freezing thawing cycles had a recovery of >90% positively buoyant spheres. The recovery of K1 was lower, around 75%. For both materials the recovery was relatively stable over time, indication that any potential breakage happened early in the experimental phase, potentially already during handling. In contrast to 25P45 and K1, the amount of positively buoyant PS decreased over time, with the largest change occurring within the first two weeks. This may

indicate that a portion of the materials are sensitive to freezing and/or thawing and once this portion is broken the remaining material is relatively resistant to further cycles of freezing and thawing.

The 25P45 material was also the most stable in long-term seawater exposures. Recoveries were high and were similar in both non-filtered and sterile filtered seawater. Interestingly, the bacterial counts in the water phase in samples being incubated for three months with 25P45 were approximately half of that of the controls. The range of the bacterial cell number determined in this study is comparable to previously reported numbers for seawater from the Trondheimsfjord and the Arctic (Ribicic et al., 2018; Brakstad et al., 2008).

Bacterial cell counts in K1 were comparable to those in 25P45, however, recovery of positively buoyant K1 was less than for 25P45. For the K1, material recovery was also lower in non-filtered seawater compared to sterile filtered seawater. As it was not possible to quantify bacterial growth on the surface of the spheres with the applied method, it remains to be determined whether this difference is due to biofouling of HGM surfaces. As glass corrosion is a known phenomenon in aqueous environments (Gin et al., 2021), it is possible that the overall low recovery (43 ± 3%) for K1 could be caused by dissolution of the material. We found that K1 was leaching a significant amount of dissolved (<0.45 μm) Si, accounting for approximately 6.4% of the originally added HGM mass after three months of incubation in sterile filtered sea water. While this cannot explain all the material loss, it should be noted that the leaching of elements was determined in sterile filtered water, where recoveries for K1 were higher (77%). It has previously been reported that the presence of microorganisms (bacterial and fungi) can affect the corrosion of glass in aqueous solutions with colonisation of mineral surfaces being selective and dependent on the mineral composition and structure (Hutchens, 2009; Weaver et al., 2021).

Corrosion of glass is generally driven by ion exchange of ionic species in the glass and in the water, hydrolysis of network forming species followed by dissolution of the hydrolysed species (Gin et al., 2021). In our study, Si was the most prominent of the analysed elements that leached from the tested materials, accounting for >5% of the added Q-Cel and K1 materials, and 1.3% of the 25P45 mass, respectively. The PS material seemed to leach more Al but much less Si than any of the other tested materials. In agreement with this, seemingly all added PS material was recovered at the end of the experiment, albeit not as positively buoyant spheres. The kind of glass used in the HGM materials thus appeared to play an important role for corrosion susceptibility. Soda-lime glass is generally less resistant to environmental impacts compared to borosilicate glass, with a typical corrosion rate of an ordinary soda–lime–silica glass reported to be <10 μm per year (Oliver et al., 2010). For HGMs featuring a wall thickness around 1 μm, corrosion could thus still be a relevant process in relatively short-term stability tests like the ones reported here.

Dissolution of elements from HGMs, and thus whether HGMs can be a relevant source of elements/nutrients to nutrient poor aquatic environments such as the Arctic Ocean should be considered. Understanding the potential effects of such releases will require more detailed studies of leaching of elements from HGMs, the possible dissolution of HGMs in natural environments and predictions using environmental modelling of release scenarios.

The results reported here give important insight into many aspects guiding the choice and/or possible specific design of HGM material for use in climate intervention. The results may also be of general interest for other applications of HGM materials.

5. Conclusion

HGMs are commercial materials and in that respect the fate and effect of their planned or accidental release into the natural environment warrants further investigation. The results of this study showed that different HGM materials have properties that affect their suitability for the proposed application in local climate intervention. Understanding the behaviour and fate of HGMs in cold environments is paramount for their possible effective and safe application in regional climate intervention for preservation of snow and ice surfaces, as suggested by Field et al. (2018). The results presented here indicate that the HGM material 25P45 is the most stable of the materials tested under conditions relevant for their application in the Arctic. Further studies of the effectiveness and environmental safety, including toxicity testing under such application should be conducted.

CRediT authorship contribution statement

Julia Farkas: Conceptualization, Data curation, Formal analysis, Investigation, Methodology, Validation, Visualization, Funding acquisition, Project administration, Resources, Writing – original draft, Writing – review & editing. **Marianne Molid:** Formal analysis, Investigation, Methodology, Writing – original draft. **Bjørn Henrik Hansen:** Conceptualization, Formal analysis, Resources, Writing – review & editing. **Tor Nordam:** Formal analysis, Writing – original draft. **Trond Nordtug:** Conceptualization, Formal analyses, Investigation, Methodology. **Patricia A. Carvalho:** Investigation. **Mimmi Throne-Holst:** Conceptualization, Funding acquisition, Project administration, Resources, Writing – original draft.

Declaration of Competing Interest

The authors declare the following financial interests/personal relationships which may be considered as potential competing interests: Julia Farkas reports financial support was provided by Arctic Ice Project.

Data availability

Data will be made available on request.

Acknowledgments

This work was financially supported by the Arctic Ice Project (https://www.arcticiceproject.org/).

Appendix A. Supplementary data

Supplementary data to this article can be found online at https://doi.org/10.1016/j.coldregions.2023.103967.

References

Bennett, A.P., Bouffard, T.J., Bhatt, U.S., 2022. Arctic Sea ice decline and geoengineering solutions: cascading security and ethical considerations. Challenges 13, 22. https://doi.org/10.3390/challe13010022.

Brakstad, O.G., Nonstad, I., Faksness, L.-G., Brandvik, P.J., 2008. Responses of microbial communities in Arctic Sea ice after contamination by crude petroleum oil. Microb. Ecol. 55, 540–552. https://doi.org/10.1007/s00248-007-9299-x.

Brakstad, O.G., Nordtug, T., Throne-Holst, M., 2015. Biodegradation of dispersed Macondo oil in seawater at low temperature and different oil droplet sizes. Mar. Pollut. Bull. 93, 144–152.

Field, L., Ivanova, D., Bhattacharyya, S., Mlaker, V., Sholtz, A., Decca, R., et al., 2018. Increasing Arctic Sea ice albedo using localized reversible geoengineering. Earth's Future 6, 882–901. https://doi.org/10.1029/2018EF000820.

Gin, S., Delaye, J.-M., Angeli, F., Schuller, S., 2021. Aqueous alteration of silicate glass: state of knowledge and perspectives. npj Mater. Degrad. 5, 42. https://doi.org/10.1038/s41529-021-00190-5.

Hutchens, E., 2009. Microbial selectivity on mineral surfaces: possible implications for weathering processes. Geomycology 23, 115–121. https://doi.org/10.1016/j.fbr.2009.10.002.

Intergovernmental Panel on Climate Change, 2018. Global Warming of 1.5°C. IPCC. https://www.ipcc.ch/sr15/.

Intergovernmental Panel on Climate Change, 2019. The ocean and the cryosphere in a Changing Climate. IPCC. https://www.ipcc.ch/srocc/.

Intergovernmental Panel on Climate Change, 2021. AR6 Climate Change 2021: The physical science basis. IPCC. https://www.ipcc.ch/report/sixth-assessment-report-working-group-i/.

Intergovernmental Panel on Climate Change, 2022. AR6 Climate Change 2022: Mitigation of Climate Change. IPCC. https://www.ipcc.ch/report/sixth-assessment-report-working-group-3/.
Keith, D., 2000. Geoengineering the climate: history and prospect. Annu. Rev. Energy Environ. 25, 245–284.
Notz, D., Stroeve, J., 2016. Observed Arctic Sea-ice loss directly follows anthropogenic CO2 emission. Science 354, 747–750. https://doi.org/10.1126/science.aag2345.
Oliver, S., Proctor, B.A., May, C.A., 2010. Degradation of glass and glass ceramics*. In: Shreir's Corrosion, pp. 2306–2318. https://doi.org/10.1016/b978-044452787-5.00177-3.
Perkins, 2019. Albedo is a simple concept that plays complicated roles in climate and astronomy. PNAS. 116 (51), 25369–25371.
Pistone, K., Eisenman, I., Ramanathan, V., 2014. Observational determination of albedo decrease caused by vanishing Arctic Sea ice. PNAS 111 (9), 3322–3326.
Ribicic, D., Netzer, R., Winkler, A., Brakstad, O.G., 2018. Microbial communities in seawater from an Arctic and a temperate Norwegian fjord and their potentials for biodegradation of chemically dispersed oil at low seawater temperatures. Mar. Pollut. Bull. 129, 308–317. https://doi.org/10.1016/j.marpolbul.2018.02.024.
Stroeve, J.C., Kattsov, V., Barrett, A., Serreze, M., Pavlova, T., Holland, M., Meier, W.N., 2012. Trends in Arctic Sea ice extent from CMIP5, CMIP3 and observations. Geophys. Res. Lett. 39, L16502. https://doi.org/10.1029/2012GL052676.
Weaver, J.L., DePriest, P.T., Plymale, A.E., Pearce, C.I., Arey, B., Koestler, R.J., 2021. Microbial interactions with silicate glasses. Npj Mater. Degrad. 5, 11. https://doi.org/10.1038/s41529-021-00153-w.